Thermal sunset diagram for scalar field theories

Tetsuo Nishikawa,* Osamu Morimatsu,† and Yoshimasa Hidaka‡
Institute of Particle and Nuclear Studies, High Energy Accelerator Research Organization, 1-1, Ooho, Tsukuba, Ibaraki, 305-0801, Japan
(Received 13 February 2003; revised manuscript received 3 July 2003; published 28 October 2003)

We study the so-called ''sunset diagram,'' which is one of two-loop self-energy diagrams, for scalar field theories at finite temperature. Explicit expressions for the real and imaginary parts of the thermal sunset diagram are obtained and they are numerically evaluated. This is done separately for the temperature independent and dependent parts of the diagram. For the former, the imaginary part is first found and the finite real part is then obtained through the imaginary part using a twice-subtracted dispersion relation. For the latter, we express it as a one-dimensional integral in terms of the bubble diagram, which is the one-loop subdiagram of the sunset diagram. As an application of our result, we study the effect of the diagram on the spectral function of the sigma meson at finite temperature in the linear sigma model, which was obtained at one-loop order previously. At high temperature where the decay $\sigma \to \pi\pi$ is forbidden, the sigma meson acquires a finite width of the order of 10 MeV by the sunset diagram while its width vanishes within the one-loop calculation. At low temperature, the spectrum does not deviate much from that at one-loop order. Possible consequences with including other two-loop diagrams are discussed.

DOI: 10.1103/PhysRevD.68.076002 PACS number(s): 11.10.Wx, 12.40.−y, 14.40.Aq, 14.40.Cs

I. INTRODUCTION

The so-called sunset diagram, which is depicted in Fig. 1, is one of two-loop self-energy diagrams. The sunset diagram appears in theories with 4-point vertices such as the $O(4)$ linear sigma model, ϕ^4 theory, and so on.

At finite temperature, two-loop self-energy diagrams have remarkable features that are not seen at zero temperature. Consider the discontinuity of the self-energy. At zero temperature, the discontinuity of one-loop diagrams is due to two-particle intermediate states and that of two-loop diagrams comes from three-particle states in addition to two-particle ones. In general, new processes appear in higher loop diagrams. However, they contribute to the discontinuity only at higher energies. On the other hand, at finite temperature new processes appear even at low energy, though the number of particles participating in the process at a given order of loops is the same as that at zero temperature. This is because some of the particles participating in the process can be those in the heat bath at finite temperature. In particular, there exist processes which are possible at arbitrary energy. Accordingly, the discontinuity of two-loop self-energies is nonvanishing in all the energy region. Therefore extending calculations to two-loop order has a meaning not just making more precision but incorporating new physics in some cases at finite temperature.

One of such cases is the spectral function for the sigma meson in the linear sigma model. The spectral function of the sigma meson at finite temperature was studied by Chiku and Hatsuda at the one-loop level [1]. The sigma meson at zero temperature has a large width due to the strong coupling with two pions. However, they found that at finite temperature the spectral function near the $\sigma \to \pi\pi$ threshold is enhanced as a typical signal of chiral phase transition. This is because, as the temperature increases, the mass of the sigma meson decreases while that of the pi meson increases due to partial restoration of chiral symmetry and, accordingly, the phase space available for the $\sigma \to \pi\pi$ decay is squeezed to zero. At finite temperature, however, there exist processes, such as the sigma meson collide with or absorb a thermal particle in the heat bath, which contribute to the discontinuity at arbitrary energy for the sigma meson, as discussed above. If we include them, the structure of the spectral function might be significantly modified. Their effects on the spectral function cannot be taken into account until we extend the calculation including two-loop self-energies.

In the quantum field theory at finite temperature, however, technology for explicit perturbative calculations of higher loop diagrams is underdeveloped. Indeed, while closed loop diagrams, which contribute to free energy, have been calculated up to the three-loop order in symmetric ϕ^4 theory [2], explicit calculations of all the two-loop self-energy diagrams in theories, symmetry-broken, e.g., ϕ^4 theory or the $O(4)$ linear sigma model, have not been completely carried out yet. Among two-loop self-energy diagrams, the sunset diagram has been investigated by some authors so far. Jeon [3], Wang and Heinz [4], and Blaizot and Iancu [5] discussed the discontinuity of the thermal sunset diagram in symmetric ϕ^4 theory and its physical interpretation in terms of elementary processes. In Ref. [3] the on-shell value of the discontinuity was also computed explicitly as a function of spatial momentum. Hees and Knoll [6] applied self-consistent Dyson re-

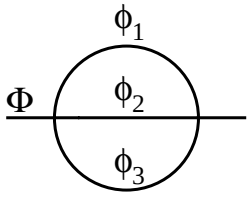

FIG. 1. ''Sunset'' diagram. We label the external particle by ''Φ'' and internal particles with mass m_i by ϕ_i.

*Electronic address: nishi@post.kek.jp
†Electronic address: osamu.morimatsu@kek.jp
‡Electronic address: hidaka@post.kek.jp

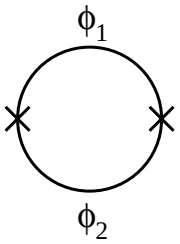

FIG. 2. ''Bubble'' diagram.

summation to symmetric ϕ^4 theory and numerically computed the sunset diagram.

In this paper, we evaluate the sunset diagram for scalar filed theories, as depicted in Fig. 1, with arbitrary internal particle's masses and external momentum. It is a first step forward to the complete two-loop analysis of the σ spectral function at finite temperature. To compute the diagram, we first rewrite it as a convolution of the one-loop diagram, the bubble diagram (see Fig. 2). The expression of the bubble diagram at finite temperature is well-known. Using the expression of the diagram, we evaluate the sunset diagram numerically. The structure of the imaginary part of the sunset diagram is also discussed. Then we study the effects of the diagram on the σ spectrum by applying a resummation technique called optimized perturbation theory [1] to the $O(4)$ linear sigma model.

This paper is organized as follows. In the second section, we summarize the expression of the ''bubble'' diagram, a one-loop subdiagram of the sunset diagram as a preparation. In the third section, we explain how we renormalize and calculate the sunset diagram. Using our result for this diagram, we study the effects of the diagram on the spectral function of σ at finite temperature in the fourth section. Finally we summarize the paper in the fifth section. In the appendixes we give a brief review of the real time formalism [7–19], which we use for the calculation of diagrams, and also discuss the structure of the imaginary part of the sunset diagram.

II. BUBBLE DIAGRAM

The ''bubble'' diagram appears as a subdiagram of the sunset diagram and therefore we need the expression of the former in the calculation of the latter. The structure of its discontinuity at finite temperature has been discussed some time ago by Weldon [20] and by now its calculation is well understood (e.g., [6]). In this section we summarize the expressions of the bubble diagram for later use.

Among the 4-components of the bubble diagram we need only the (1,1) component since the sunset diagram does not have any internal vertices. The (1,1) component of the bubble diagram for scalar particles is given by

$$i\mathcal{I}_{\rm bub}(p;m_1,m_2)_{11}=i\int\frac{{\rm d}^4k}{(2\pi)^4}i\Delta_{11}^F(p+k;m_1)i\Delta_{11}^F(k;m_2), \tag{1}$$

where $i\Delta_{11}^F(p;m)$ is the (1,1) component of the free propagator of a scalar particle with mass m given in Eq. (A1). Equation (1) can be expressed as the sum of terms with different numbers of Bose-Einstein factors, n:

$$i\mathcal{I}_{\rm bub}(p;m_1,m_2)_{11}=iI^{(2)}(p^2;m_1,m_2)+[iF^{(2)}(p;m_1,m_2)+(1\leftrightarrow 2)]+iF^{(3)}(p;m_1,m_2). \tag{2}$$

Each term in the right-hand side is, respectively, given by

$$iI^{(2)}(p^2;m_1,m_2)=i\int\frac{{\rm d}^4k}{(2\pi)^4}\frac{i}{(p+k)^2-m_1^2+i\eta}\frac{i}{k^2-m_2^2+i\eta}, \tag{3}$$

$$iF^{(2)}(p;m_1,m_2)=i\int\frac{{\rm d}^4k}{(2\pi)^4}\frac{i}{(p+k)^2-m_1^2+i\eta}n(k_0)2\pi\delta(k^2-m_2^2), \tag{4}$$

$$iF^{(3)}(p;m_1,m_2)=i\int\frac{{\rm d}^4k}{(2\pi)^4}n(p_0+k_0)\times 2\pi\delta[(p+k)^2-m_1^2]n(k_0)2\pi\delta(k^2-m_2^2). \tag{5}$$

The T-independent part $I^{(2)}$ is given in textbooks [21]. In d-dimension it is given by

$$iI^{(2)}(p^2;m_1,m_2)=\frac{-1}{16\pi^2}\left(-\frac{1}{\bar{\epsilon}}+x_+\ln\frac{m_1^2}{\kappa^2}-x_-\ln\frac{m_2^2}{\kappa^2}-2-I\right), \tag{6}$$

where κ is the renormalization point and $1/\bar{\epsilon}$ and $x_\pm$ are

$$\frac{1}{\bar{\epsilon}}\equiv\frac{1}{\epsilon}-\gamma+\ln 4\pi\quad[\epsilon=(4-d)/2,\quad\gamma:\ \text{Euler constant}], \tag{7}$$

$$x_\pm\equiv\pm\frac{1}{2}+\frac{m_1^2-m_2^2}{2p^2}. \tag{8}$$

I is given by

$$I=\begin{cases}\sqrt{C}\left[\ln\dfrac{(x_+-\sqrt{C})(x_-+\sqrt{C})}{(x_--\sqrt{C})(x_++\sqrt{C})}+i2\pi\right] & \text{for} \quad p^2>(m_1+m_2)^2\\ -2\sqrt{D}\left[\arctan\dfrac{x_+}{\sqrt{D}}-\arctan\dfrac{x_-}{\sqrt{D}}\right] & \text{for} \quad (m_1-m_2)^2<p^2<(m_1+m_2)^2\\ \sqrt{C}\ln\dfrac{(\sqrt{C}-x_+)(\sqrt{C}+x_-)}{(\sqrt{C}-x_-)(\sqrt{C}+x_+)} & \text{for} \quad p^2<(m_1-m_2)^2,\end{cases} \tag{9}$$

where C and D are

$$C\equiv\frac{1}{4}\left[1-\frac{(m_1+m_2)^2}{p^2}\right]\left[1-\frac{(m_1-m_2)^2}{p^2}\right], \quad D\equiv -C. \tag{10}$$

We see from Eqs. (3) and (9) that the imaginary part of $iI^{(2)}$ is nonvanishing for $p^2>(m_1+m_2)^2$.

Let us next turn to the T-dependent part, $iF^{(2)}$ and $iF^{(3)}$. The imaginary part of $iF^{(2)}(p;m_1,m_2)$ is given analytically as follows:

(1) For $p^2>(m_1+m_2)^2$ or $0<p^2<(m_1-m_2)^2$,

$$\mathrm{Im}\, iF^{(2)}(p;m_1,m_2)=\frac{1}{16\pi|\mathbf{p}|}\frac{1}{\beta}\ln\left|\frac{1-e^{-\beta\omega_+}}{1-e^{-\beta\omega_-}}\right|. \tag{11}$$

(2) For $(m_1-m_2)^2<p^2<(m_1+m_2)^2$,

$$\mathrm{Im}\, iF^{(2)}(p;m_1,m_2)=0. \tag{12}$$

(3) For $p^2<0$,

$$\mathrm{Im}\, iF^{(2)}(p;m_1,m_2)=\frac{1}{16\pi|\mathbf{p}|}\frac{-1}{\beta}\ln|(1-e^{-\beta\omega_+})(1-e^{-\beta\omega_-})|. \tag{13}$$

Here,

$$\omega_\pm=\frac{1}{2}\left|\sqrt{\left(1+\frac{m_2^2-m_1^2}{p^2}\right)^2}|p_0| \pm\sqrt{\left[1-\frac{(m_2+m_1)^2}{p^2}\right]\left[1-\frac{(m_1-m_2)^2}{p^2}\right]}|\mathbf{p}|\right|. \tag{14}$$

$iF^{(3)}$ has only an imaginary part and is given as follows:

(1) For $p^2>(m_1+m_2)^2$,

$$iF^{(3)}(p;m_1,m_2)=\frac{i}{8\pi|\mathbf{p}|\beta}\frac{1}{e^{\beta|p_0|}-1}\times\ln\left|\frac{1-e^{-\beta\omega_+}}{1-e^{-\beta\omega_-}}\frac{e^{\beta(|p_0|-\omega_-)}-1}{e^{\beta(|p_0|-\omega_+)}-1}\right|. \tag{15}$$

(2) For $(m_1-m_2)^2<p^2<(m_1+m_2)^2$,

$$iF^{(3)}(p;m_1,m_2)=0. \tag{16}$$

(3) For $0<p^2<(m_1-m_2)^2$,

$$iF^{(3)}(p;m_1,m_2)=\frac{i}{8\pi|\mathbf{p}|\beta}\cdot\frac{1}{e^{\beta|p_0|}-1}\left[\ln\left|\frac{1-e^{-\beta\omega_+}}{1-e^{-\beta\omega_-}}\right|-e^{\beta|p_0|}\ln\left|\frac{1-e^{-\beta(|p_0|+\omega_+)}}{1-e^{-\beta(|p_0|+\omega_-)}}\right|\right]. \tag{17}$$

(4) For $p^2<0$,

$$iF^{(3)}(p;m_1,m_2)=\frac{i}{8\pi|\mathbf{p}|\beta}\left\{\frac{1}{e^{-\beta|p_0|}-1}[-\ln|1-e^{-\beta\omega_+}|+e^{-\beta|p_0|}\ln|1-e^{-\beta(\omega_+-|p_0|)}|]+\frac{1}{e^{\beta|p_0|}-1}[-\ln|1-e^{-\beta\omega_-}|+e^{\beta|p_0|}\ln|1-e^{-\beta(\omega_-+|p_0|)}|]\right\}. \tag{18}$$

In Eqs. (15)–(18), $\omega_\pm$ are given by Eq. (14) with m_1 and m_2 replaced by $\max\{m_1,m_2\}$ and $\min\{m_1,m_2\}$, respectively, since $F^{(3)}(p;m_1,m_2)$ is symmetric with respect to m_1 and m_2 by definition.

It should be noted that the T-dependent part has two cuts in the complex p^2 plane: one starts from $p^2=(m_1+m_2)^2$ to the right along the real axis and the other from $p^2=(m_1-m_2)^2$ to the left.

The real part of $iF^{(2)}$ can be expressed as a one-dimensional integral:

$$\mathrm{Re}\, iF^{(2)}(p;m_1,m_2) = \frac{1}{16\pi^2|\mathbf{p}|}\int_{m_2}^{\infty} d\omega n(\omega)\mathcal{P}\ln\left|\frac{(p^2+2p_0\omega-2|\mathbf{p}|\sqrt{\omega^2-m_2^2}+m_2^2-m_1^2)(p^2-2p_0\omega-2|\mathbf{p}|\sqrt{\omega^2-m_2^2}+m_2^2-m_1^2)}{(p^2+2p_0\omega+2|\mathbf{p}|\sqrt{\omega^2-m_2^2}+m_2^2-m_1^2)(p^2-2p_0\omega+2|\mathbf{p}|\sqrt{\omega^2-m_2^2}+m_2^2-m_1^2)}\right|, \tag{19}$$

where $\mathcal{P}$ stands for the prescription of Cauchy's principal value. The integration in Eq. (19) will be carried out numerically.

III. CALCULATION OF THE THERMAL SUNSET DIAGRAM

In this section, we explain how to renormalize and calculate the thermal sunset diagram.

The (1,1) component of the sunset diagram shown in Fig. 1 is given by

$$\mathcal{I}_{\mathrm{sun}}(k;m_1,m_2,m_3)_{11} = \int \frac{d^4p}{(2\pi)^4} i\Delta_{11}^F(p;m_1) \times \int \frac{d^4q}{(2\pi)^4} i\Delta_{11}^F(q;m_2) i\Delta_{11}^F(k-p-q;m_3). \tag{20}$$

We decompose Eq. (20) into terms with and without Bose-Einstein factors, which we denote by $\mathcal{I}^{\mathrm{th}}_{\mathrm{sun}}(k^2;m_1,m_2,m_3)_{11}$ and $\mathcal{I}^{\mathrm{vac}}_{\mathrm{sun}}(k;m_1,m_2,m_3)_{11}$, respectively:

$$\mathcal{I}_{\mathrm{sun}}(k;m_1,m_2,m_3)_{11} = \mathcal{I}^{\mathrm{vac}}_{\mathrm{sun}}(k^2;m_1,m_2,m_3)_{11} + \mathcal{I}^{\mathrm{th}}_{\mathrm{sun}}(k;m_1,m_2,m_3)_{11}. \tag{21}$$

They can be written as

$$\mathcal{I}^{\mathrm{vac}}_{\mathrm{sun}}(k^2;m_1,m_2,m_3)_{11} = \int \frac{d^4p}{(2\pi)^4}\frac{i}{p^2-m_1^2+i\eta} I^{(2)}[(k-p)^2;m_2,m_3], \tag{22}$$

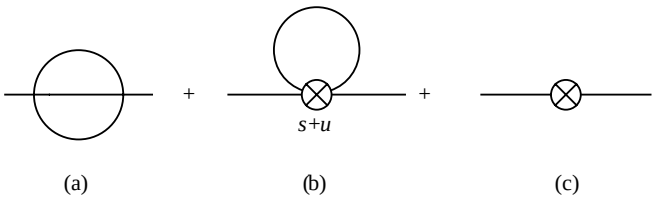

FIG. 3. Renormalization of the sunset diagram. The diagram labeled (a) is a bare sunset diagram. The diagrams labeled (b) and (c) cancel the sub- and overall divergences in (a), respectively. (b) is generated from the counterterm which removes the divergence of the one-loop four-point vertex function in s and u channels (see Fig. 4.).

$$\mathcal{I}^{\mathrm{th}}_{\mathrm{sun}}(k;m_1,m_2,m_3)_{11} = \int \frac{d^4p}{(2\pi)^4}\frac{i}{p^2-m_1^2+i\eta} \times[(F^{(2)}(k-p;m_2,m_3)+(2\leftrightarrow 3)) + F^{(3)}(k-p;m_2,m_3)] + \int \frac{d^4p}{(2\pi)^4} n(p_0) \times 2\pi\delta(p^2-m_1^2)[I^{(2)}((k-p)^2;m_2,m_3) + (F^{(2)}(k-p;m_2,m_3)+(2\leftrightarrow 3)) + F^{(3)}(k-p;m_2,m_3)]. \tag{23}$$

These expression are obtained by expressing the second integral in Eq. (20) in terms of $I^{(2)}$, $F^{(2)}$, and $F^{(3)}$ given in the previous section. We rewrite the integrand of the first term in the T-dependent part of Eq. (23) so that it becomes the same form as that in the second term, i.e., (a delta function)$\times$(some functions). This can be done by recombining the two factors in the integrand of $F^{(2)}(k-p;m_2,m_3)+(2\leftrightarrow 3)$ and $F^{(3)}(k-p;m_2,m_3)$, the T-independent part and T-dependent part of $i\Delta_{11}^F$:

$$\mathcal{I}^{\mathrm{th}}_{\mathrm{sun}}(k;m_1,m_2,m_3)_{11} = \int \frac{d^4p}{(2\pi)^4}\{n(p_0)2\pi\delta(p^2-m_1^2)[I^{(2)}((k-p)^2;m_2,m_3) + (F^{(2)}(k-p;m_2,m_3)+(2\leftrightarrow 3)) + F^{(3)}(k-p;m_2,m_3)] + n(p_0)2\pi\delta(p^2-m_3^2)[I^{(2)}((k-p)^2;m_1,m_3)+F^{(2)}(k-p;m_1,m_3)] + n(p_0)2\pi\delta(p^2-m_3^2)I^{(2)}((k-p)^2;m_1,m_2)\}. \tag{24}$$

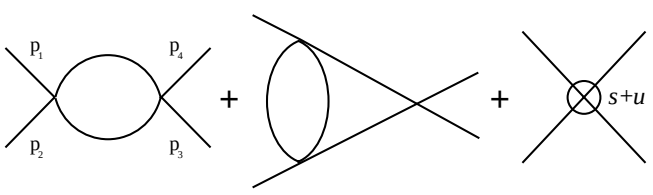

FIG. 4. Four-point vertex function at one-loop order in s and u channels in ϕ^4 theory. The last diagram stands for the one generated from the counterterm, $-\lambda/4!C\phi^4$, in Eq. (25).

It is well known that the vacuum part, $\mathcal{I}^{\rm vac}_{\rm sun}(k^2;m_1,m_2,m_3)_{11}$, is divergent. The thermal part, $\mathcal{I}^{\rm vac}_{\rm sun}(k;m_1,m_2,m_3)_{11}$, is also divergent because it includes $I^{(2)}$. We first discuss how they are renormalized.

A. Renormalization

At finite temperature the sunset diagram is renormalized in the same way as at zero temperature by combining the three diagrams given in Fig. 3.

In order to be specific we take the ϕ^4 theory:

$$\mathcal{L}=\frac{1}{2}(\partial_\mu\phi)^2-\frac{1}{2}m^2\phi^2-\frac{\lambda}{4!}\phi^4+\frac{1}{2}A(\partial_\mu\phi)^2-\frac{1}{2}Bm^2\phi^2 - \frac{\lambda}{4!}C\phi^4, \tag{25}$$

where the last three terms are counterterms.

The expressions of the three diagrams, (a), (b), and (c) in Fig. 3, are as follows, respectively:

$$\Pi^{(a)}=\frac{(-i\lambda)^2}{6}\int\frac{d^4p}{(2\pi)^4}i\Delta^F_{11}(p;m) \times\int\frac{d^4q}{(2\pi)^4}i\Delta^F_{11}(q;m)i\Delta^F_{11}(k-p-q;m), \tag{26}$$

$$\Pi^{(b)}=\frac{1}{2}\lambda C\int\frac{d^4p}{(2\pi)^4}i\Delta^F_{11}(p;m), \tag{27}$$

$$\Pi^{(c)}=-iBm^2. \tag{28}$$

C is determined so as to cancel the divergence of the one-loop four-point vertex function in s and u channels at zero temperature as depicted in Fig. 4.

$$\frac{(-i\lambda)^2}{2}[I^{(2)}(s;m,m)+I^{(2)}(u;m,m)]-i\lambda C=\text{finite}, \tag{29}$$

where $s=(p_1+p_2)^2$ and $u=(p_1-p_4)^2$.

It is well known that the T-independent part of the sunset diagram is renormalized by combining $\Pi^{(a)}$, $\Pi^{(b)}$, and $\Pi^{(c)}$ [30]. Here, we demonstrate that the divergence of its T-dependent part also cancels in $\Pi^{(a)}$ and $\Pi^{(b)}$ ($\Pi^{(c)}$ is T-independent). The T-dependent part of $\Pi^{(a)}$ and $\Pi^{(b)}$ is given, respectively, by

$$\Pi^{(a)}=\frac{(-i\lambda)^2}{6}\int\frac{d^4p}{(2\pi)^4}n(p_0)2\pi\delta(p^2-m^2) \times[3iI^{(2)}((k-p)^2;m,m)+3iF^{(2)}(k-p;m,m) + iF^{(3)}(k-p;m,m)], \tag{30}$$

$$\Pi^{(b)}=\frac{1}{2}\lambda C\int\frac{d^4p}{(2\pi)^4}n(p_0)2\pi\delta(p^2-m^2). \tag{31}$$

The divergence in Eq. (31) comes only from $I^{(2)}$. Then, the divergence in the sum of the T-dependent part, $\Pi^{(a)}+\Pi^{(b)}$, becomes

$$\int\frac{d^4p}{(2\pi)^4}n(p_0)2\pi\delta(p^2-m^2) \times\left\{\frac{(-i\lambda)^2}{2}iI^{(2)}[(k-p)^2;m,m]+\frac{1}{2}\lambda C\right\}=\text{finite} \tag{32}$$

from Eq. (29).

This clearly shows that the T-independent coupling constant renormalization at one-loop order automatically renormalizes the T-dependent part of the sunset diagram. This also means that the T-dependent sunset diagram depends on the scheme adopted for the calculation of the T-independent coupling constant at one-loop order.

In this paper we adopt the $\overline{\rm MS}$ scheme. In the $\overline{\rm MS}$ scheme, C is given by

$$C_{\overline{\rm MS}}=\frac{\lambda}{16\pi^2}\frac{1}{\bar{\epsilon}} \tag{33}$$

and

$$\Pi^{(a)}+\Pi^{(b)}=\frac{(-i\lambda)^2}{6}\int\frac{d^4p}{(2\pi)^4}n(p_0)2\pi\delta(p^2-m^2) \times[3i\tilde{I}^{(2)}((k-p)^2;m,m)+3iF^{(2)}(k-p;m,m) + iF^{(3)}(k-p;m,m)], \tag{34}$$

where $\tilde{I}^{(2)}$ denotes $I^{(2)}$ with the $1/\bar{\epsilon}$ term subtracted.

Also in other theories the renormalization of the T-dependent part of the sunset diagram can be carried out in a similar way by subtracting the divergence in the subdiagram. If we adopt the $\overline{\rm MS}$ scheme, it amounts to taking out the $1/\bar{\epsilon}$ term.

Next, we show how we calculate the finite T-independent and T-dependent parts of the sunset diagram separately.

B. *T*-independent part

The *T*-independent part of sunset type diagrams has been calculated by several authors [6,22] so far. In this paper we calculate its finite part by using a dispersion relation. The method which we employ is basically the same as that by Hees and Knoll [6]. We first find the imaginary part of $i\mathcal{I}^{\rm vac}_{\rm sun}(k^2;m_1,m_2,m_3)_{11}$ and then compute the finite real part using the obtained imaginary part, *via* the twice-subtracted dispersion relation.

In order to calculate the imaginary part of $i\mathcal{I}^{\rm vac}_{\rm sun}(k^2;m_1,m_2,m_3)_{11}$, we substitute a dispersion relation for $iI^{(2)}[(k-p)^2;m_2,m_3]$:

$$iI^{(2)}[(k-p)^2;m_2,m_3] = \frac{1}{\pi}\int_{(m_2+m_3)^2}^{\infty} dM^2 \frac{\mathrm{Im}\, iI^{(2)}(M^2;m_2,m_3)}{M^2-(k-p)^2-i\eta}, \tag{35}$$

into Eq. (22). Then, we obtain

$$\begin{aligned} i\mathcal{I}^{\rm vac}_{\rm sun}(k^2;m_1,m_2,m_3)_{11} &= \frac{1}{\pi}\int_{(m_2+m_3)^2}^{\infty} dM^2\, \mathrm{Im}\, iI^{(2)}(M^2;m_2,m_3)\cdot i \\ &\times \int \frac{d^4p}{(2\pi)^4}\frac{i}{p^2-m_1^2+i\eta}\frac{i}{(k-p)^2-M^2+i\eta} \\ &= \frac{1}{\pi}\int_{(m_2+m_3)^2}^{\infty} dM^2\, \mathrm{Im}\, iI^{(2)}(M^2;m_2,m_3) \\ &\times iI^{(2)}(k^2;m_1,M). \end{aligned} \tag{36}$$

We take the imaginary part of this equation:

$$\begin{aligned} \mathrm{Im}\, i\mathcal{I}^{\rm vac}_{\rm sun}(k^2;m_1,m_2,m_3)_{11} &= \frac{1}{\pi}\int_{(m_2+m_3)^2}^{\infty} dM^2\, \mathrm{Im}\, iI^{(2)}(M^2;m_2,m_3) \\ &\times \mathrm{Im}\, iI^{(2)}(k^2;m_1,M). \end{aligned} \tag{37}$$

Using the expression for $\mathrm{Im}\, iI^{(2)}(p^2;m,m_2)$ we can easily evaluate Eq. (37) numerically.

Next we turn to the real part. In order to calculate its finite part, we use the twice-subtracted dispersion relation:

$$\begin{aligned} \mathrm{Re}\, i\tilde{\mathcal{I}}^{\rm vac}_{\rm sun}(k^2;m_1,m_2,m_3)_{11} &\equiv \mathrm{Re}\Bigg\{ i\mathcal{I}^{\rm vac}_{\rm sun}(k^2;m_1,m_2,m_3)_{11} - i\mathcal{I}^{\rm vac}_{\rm sun}(0;m_1,m_2,m_3)_{11} \\ &- k^2\left[\frac{\partial}{\partial k^2} i\mathcal{I}^{\rm vac}_{\rm sun}(k^2;m_1,m_2,m_3)_{11}\right]_{k^2=0}\Bigg\} \\ &= \frac{k^4}{\pi}\int_{(m_1+m_2+m_3)^2}^{\infty} dM^2 \mathcal{P}\frac{\mathrm{Im}\, i\mathcal{I}^{\rm vac}_{\rm sunset}(M^2;m_1,m_2,m_3)}{M^4(M^2-k^2)}. \end{aligned} \tag{38}$$

As discussed above, each term in the left-hand side is divergent but the right-hand side is finite and remains unchanged by renormalization. Using the results for $\mathrm{Im}\, i\mathcal{I}^{\rm vac}_{\rm sun}(M^2;m_1,m_2,m_3)$ we calculate Eq. (38). This is done by splitting the integrand of Eq. (38) into the singular term, $\propto 1/M^2-k^2$, and the nonsingular term. The integration of the singular term is obtained analytically while that of the nonsingular term is calculated numerically with the standard method.

After $\mathrm{Re}\, i\tilde{\mathcal{I}}^{\rm vac}_{\rm sun}(m^2_{\rm phys};m_1,m_2,m_3)_{11}$ is subtracted, Eq. (38) coincides with that in the modified minimal subtraction ($\overline{\rm MS}$) scheme up to an irrelevant overall factor.

C. *T*-dependent part

After renormalizing in $\overline{\rm MS}$ scheme, and putting $k=(k_0,\mathbf{0})$, Eq. (24) is reduced to

$$\begin{aligned} i\tilde{\mathcal{I}}^{\rm th}_{\rm sun}(k_0,\mathbf{0};m_1,m_2,m_3)_{11} = \frac{1}{4\pi^2}\sum_{\tau=\pm}\Bigg\{ &\int_{m_1}^{\infty} d\omega n(\omega)\sqrt{\omega^2-m_1^2}\, i[\tilde{I}^{(2)}((k_0+\tau\omega)^2-(\omega^2-m_1^2);m_2,m_3) \\ &+ (F^{(2)}(k_0+\tau\omega,\sqrt{\omega^2-m_1^2};m_2,m_3)+(2\leftrightarrow 3))+F^{(3)}(k_0+\tau\omega,\sqrt{\omega^2-m_1^2};m_2,m_3)] \\ &+ \int_{m_2}^{\infty} d\omega n(\omega)\sqrt{\omega^2-m_2^2}\, i[\tilde{I}^{(2)}((k_0+\tau\omega)^2-(\omega^2-m_2^2);m_1,m_3)+F^{(2)}(k_0+\tau\omega, \\ &\sqrt{\omega^2-m_2^2};m_1,m_3)]+\int_{m_3}^{\infty} d\omega n(\omega)\sqrt{\omega^2-m_3^2}\cdot i\tilde{I}^{(2)}((k_0+\tau\omega)^2-(\omega^2-m_3^2);m_1,m_2)\Bigg\}. \end{aligned} \tag{39}$$

Using the expressions of $I^{(2)}$ with the divergence subtracted, $F^{(2)}$ and $F^{(3)}$, we can evaluate the real and imaginary parts of Eq. (39) numerically. Each term in the T-dependent part has the following form:

$$A_3 \equiv \frac{1}{4\pi^2}\int_{m_1}^{\infty} dE\, n(E)\sqrt{E^2-m_1^2}\,[A_2(\omega+E, \sqrt{E^2-m_1^2};m_2,m_3)+A_2(\omega-E,\sqrt{E^2-m_1^2};m_2,m_3)], \tag{40}$$

where $A_2(p_0,|\vec{p}|,m_2,m_3)$ stands for the one-loop self-energy integral, $iI^{(2)}$, $iF^{(2)}$, or $iF^{(3)}$. The derivative of the integrand is discontinuous at E which corresponds to the branch point for $A_2(p_0,|\vec{p}|,m_2,m_3)$, i.e., $p^2=(m_2+m_3)^2$ or $p^2=(m_2-m_3)^2$. Therefore we separate the integral region into some intervals, which correspond to $p^2<(m_2-m_3)^2$, $(m_2-m_3)^2<p^2<(m_2+m_3)^2$, and $(m_2+m_3)^2<p^2$, for each term in Eq. (40). In each interval the integration can be carried out by the standard method.

IV. CONTRIBUTION OF THE THERMAL SUNSET DIAGRAM TO THE SPECTRAL FUNCTION OF σ AT FINITE TEMPERATURE

The purpose of this section is to see how two-loop diagrams affect observables by evaluating the contribution of the thermal sunset diagram to the sigma meson spectral function at finite temperature in the linear sigma model.

It is known that naive perturbation theory breaks down at $T\neq 0$, and resummation of higher orders is necessary [23–27]. We adopt here a resummation technique called optimized perturbation theory (OPT) [1]. We first briefly review the procedure of OPT applied to the $O(4)$ linear sigma model. The original linear sigma model Lagrangian is as follows:

$$\mathcal{L}=\frac{1}{2}[(\partial_\mu\phi_i)^2-\mu^2\phi_i^2]-\frac{\lambda}{4!}(\phi_i^2)^2+h\phi_0+\text{counterterms}, \tag{41}$$

where $\phi_i=(\sigma,\vec{\pi})$ and $h\phi_0$ being the explicitly symmetry breaking term. For the renormalized couplings μ^2, λ, and h and the renormalization point κ we use the values determined in [1]: $\mu^2=-(283\ \text{MeV})^2$, $\lambda=73.0$, $h=(123\ \text{MeV})^3$, and $\kappa=255$ MeV.

In OPT one adds and subtracts a new mass term with the mass m to the Lagrangian. Thus we have

$$\mathcal{L}=\frac{1}{2}[(\partial_\mu\phi_i)^2-m^2\phi_i^2]+\frac{1}{2}\chi\phi_i^2-\frac{\lambda}{4!}(\phi_i^2)^2+h\phi_0 + (\text{counterterm}), \tag{42}$$

where $\chi\equiv m^2-\mu^2$. The idea of OPT is reorganization of perturbation theory: one treats the added one as a tree-level mass term while the subtracted one as perturbation.

When the spontaneous symmetry breaking takes place, tree level masses of π and σ read, respectively,

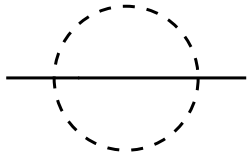

FIG. 5. The sunset diagram for σ. Solid and dashed lines correspond to σ and π, respectively.

$$m_{0\pi}^2=m^2+\frac{\lambda}{6}\xi^2, \quad m_{0\sigma}^2=m^2+\frac{\lambda}{2}\xi^2, \tag{43}$$

where ξ is the vacuum expectation value of σ and determined by the stationary condition for the thermal effective action $V(\xi,T,m^2)$ [1]:

$$\frac{\partial V(\xi,T,m^2)}{\partial\xi}=0. \tag{44}$$

Note that the derivative with respect to ξ does not act on m^2.

If Green's functions are calculated in all orders in OPT, they should not depend on the arbitrary mass m. However, if one truncates perturbation series at a certain order they depend on it. One can determine this arbitrary parameter so that the correction terms are as small as possible. We adopt the following condition [1]:

$$\Pi_\pi(k^2=m_{0\pi}^2)+\Pi_\pi(k=0;T)=0, \tag{45}$$

where the first and second terms are, respectively, the T independent part and T dependent part of the one-loop self-energy of pion.

Let us now turn to the discussion on the spectral function of σ defined by the imaginary part of the propagator:

$$\rho_\sigma(k_0,\mathbf{k}) = -\frac{1}{\pi}\frac{\text{Im}\,\overline{\Pi}_\sigma(k_0,\mathbf{k})}{[k^2-m_{0\sigma}^2-\text{Re}\,\overline{\Pi}_\sigma(k_0,\mathbf{k})]^2+[\text{Im}\,\overline{\Pi}_\sigma(k_0,\mathbf{k})]^2}. \tag{46}$$

Here $\overline{\Pi}_\sigma(k_0,\mathbf{k})$ is the self-energy of σ. Its real and imaginary parts are related with (1,1) component, Π_σ^{11}, *via* Eqs. (A13) and (A14).

As was already mentioned, the spectral function at one-loop order was studied by Chiku and Hatsuda [1]. We want to see how the spectral function at one-loop order is modified by adding the thermal sunset diagram. Thus we take

$$\Pi_\sigma^{11}(k_0,\mathbf{k})=\Pi_\sigma^{11}(k_0,\mathbf{k})_{\text{one-loop}}+\Pi_\sigma^{11}(k_0,\mathbf{k})_{\text{sun}}. \tag{47}$$

The first term is the renormalized one-loop self-energy calculated in [1]. The second term is the renormalized sunset diagram depicted in Fig. 5 and given by

$$\Pi_\sigma^{11}(k_0,\mathbf{k})_{\text{sun}}=-\frac{\lambda^2}{6}i\mathcal{I}_{\text{sun}}(k_0,\mathbf{k};m_{0\pi},m_{0\pi},m_{0\sigma})_{11}. \tag{48}$$

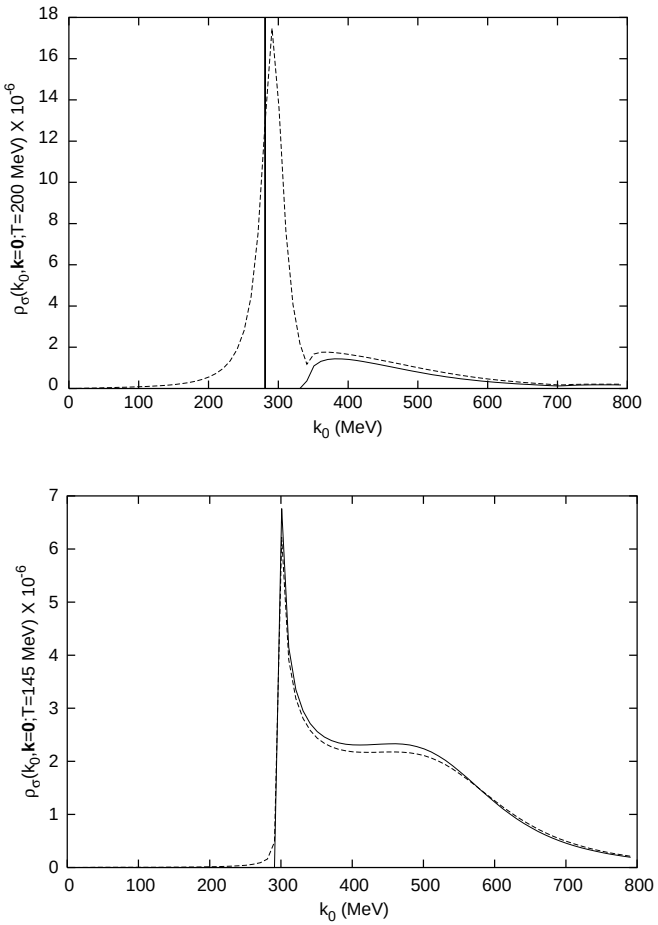

FIG. 6. Spectral function of the σ meson $\rho_\sigma(k_0,\mathbf{k}=\mathbf{0})$ at $T=200$ MeV (upper panel) and $T=145$ MeV (lower panel). The solid line corresponds to ρ_σ at one-loop order and the dashed line to that with one-loop self-energy and the sunset diagram.

We show $\rho_\sigma(k_0,\mathbf{k}=\mathbf{0})$ at $T=200$ MeV and $T=145$ MeV in Fig. 6. At $T=200$ MeV, the spectral function at one-loop order consists of a δ-function peak for σ and a continuum. By including the sunset diagram σ acquires a width of the order of 10 MeV. At lower temperature, $T=145$ MeV, an enhancement of the spectrum near the threshold is observed at one-loop order. When we include the sunset diagram, this feature is not lost.

Let us next discuss the above results. At high temperature ($T=200$ MeV), the mass of σ is smaller than twice the pion mass and the decay $\sigma\to\pi\pi$ is forbidden. As a result, within the one-loop calculation σ has zero width. However, at finite temperature σ can interact with thermal particles in a heat bath and change into other states. Among such processes, those which are taken into account by including the sunset diagram are represented in Fig. 9 with $(\Phi,\phi_1,\phi_2,\phi_3)$ assigned to, for example, (σ,σ,π,π). The processes which correspond to (a) and (b) in Fig. 9 are possible for $k_0>2m_{0\pi}+m_{0\sigma}$. This affects the spectrum at high energy. (c) and (d) in Fig. 9 drop off for positive k_0. (e) and (f) affect the spectrum at low energy since they are possible for $k_0<m_{0\sigma}-2m_{0\pi}$. The processes which correspond to (g) and (h) in Fig. 9 are shown in Fig. 7. They are the most important and

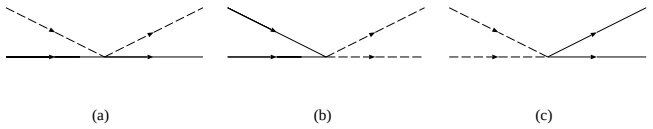

FIG. 7. The processes which are allowed at all positive k_0 contained in the imaginary part of the sunset diagram for σ (Fig. 5).

give a finite width to σ, since they are allowed at arbitrary positive k_0. However, we observe that their effects at lower temperature ($T=145$ MeV) are small. The reason is traced back to Eq. (B6). The term representing the probabilities for (g) and (h) in Fig. 9 is the fourth term. That integral at lower temperature is suppressed due to the statistical weight, since at lower temperature the masses of σ and π are large.

Finally, we note that, as a consequence of the nonvanishing imaginary part of the sunset diagram, the spectral function is also nonvanishing in the entire range of k_0.

V. SUMMARY AND PERSPECTIVE

We have studied the sunset diagram for scalar field theories at finite temperature in the real time formalism. We have explained how we can reduce it to an expression written in terms of one-loop self-energy integrals, which can be easily evaluated numerically.

As an application of the result, we have demonstrated how the spectral function of σ at finite T at one-loop order is modified when we include the thermal sunset diagram. At high temperature, where $\sigma\to\pi\pi$ is forbidden, σ acquires a finite width of the order of 10 MeV due to collisions with thermal particles in the heat bath while σ does not have a width at one-loop order. At lower temperature the spectrum is almost unchanged.

Finally, we comment on the effect of other two-loop diagrams on the spectral function. We have seen that the threshold enhancement, which was first found in the one-loop calculation, is retained if we include the sunset diagram. However, in the present calculation the effect of the thermal width of π in the $\sigma\to\pi\pi$ decay is not included. This is taken into account by including the diagrams such as shown in Fig. 8, in which an internal π changes into σ absorbing a thermal π in the heat bath.

In the one-loop calculation, π has a width, $\Gamma_\pi=50$ MeV, at the temperature, $T=145$ MeV, at which the threshold enhancement is observed for σ. If we include this effect as a constant complex mass shift for π in the one-loop self-energy for σ, we expect σ to acquire a width twice that for π, i.e., $\Gamma_\sigma=2\Gamma_\pi$ [28]. This implies that when the two-loop diagrams such as Fig. 8 are included the spectral function for σ would be significantly modified with the width of

FIG. 8. Two-loop self-energy diagram in which internal π changes into σ by absorbing thermal π in the heat bath.

about 100 MeV. The calculations of those diagrams are now in progress [29].

ACKNOWLEDGMENTS

The authors would like to thank M. Ohtani for a useful discussion. This work was partially supported by Grants-in-Aid of the Japanese Ministry of Education, Science, Sports, Culture and Technology (No. 06572).

APPENDIX A: BRIEF REVIEW OF THE REAL TIME FORMALISM

For the calculations of thermal Feynman diagrams we adopt the real time formalism throughout this paper. We briefly review the formalism in this appendix.

In the real time formalism propagators are given by 2×2 matrices. The 4-components of the free propagator of a scalar particle with mass m are given by [19]

$$i\Delta_{11}^F(k;m)=\frac{i}{k^2-m^2+i\eta}+n(k_0)2\pi\delta(k^2-m^2), \tag{A1}$$

$$i\Delta_{12}^F(k;m)=e^{\sigma k_0}[n(k_0)+\theta(-k_0)]2\pi\delta(k^2-m^2), \tag{A2}$$

$$i\Delta_{21}^F(k;m)=e^{-\sigma k_0}[n(k_0)+\theta(k_0)]2\pi\delta(k^2-m^2), \tag{A3}$$

$$i\Delta_{22}^F(k;m)=\frac{-i}{k^2-m^2-i\eta}+n(k_0)2\pi\delta(k^2-m^2), \tag{A4}$$

where $n(k_0)$ is the Bose-Einstein distribution function at temperature $T\equiv 1/\beta$:

$$n(k_0)=\frac{1}{\exp(\beta|k_0|)-1}. \tag{A5}$$

Off-diagonal elements depend on a free parameter σ. In this paper we make the symmetrical choice $\sigma=\beta/2$, leading to

$$i\Delta_{12}^F(k;m)=i\Delta_{21}^F(k;m)=e^{\beta|k_0|/2}n(k_0)2\pi\delta(k^2-m^2). \tag{A6}$$

We denote the matrix of the full propagator by

$$\tilde{\Delta}(k;m)=\begin{pmatrix}\Delta_{11}(k;m) & \Delta_{12}(k;m)\\ \Delta_{21}(k;m) & \Delta_{22}(k;m)\end{pmatrix}. \tag{A7}$$

Each component is the solution of the Schwinger-Dyson equation:

$$\Delta_{ab}(k;m)=\Delta_{ab}^F(k;m)+\Delta_{ac}^F(k;m)\Pi_{cd}(k)\Delta_{db}(k;m), \tag{A8}$$

where $\Pi_{cd}(k)$ is the self-energy.

The following matrix

$$U(k)=\begin{pmatrix}\sqrt{1+n(k_0)} & \sqrt{n(k_0)}\\ \sqrt{n(k_0)} & \sqrt{1+n(k_0)}\end{pmatrix}, \tag{A9}$$

"diagonalizes" the free propagator:

$$U(k)^{-1}\begin{pmatrix}\Delta_{11}^F(k;m) & \Delta_{12}^F(k;m)\\ \Delta_{21}^F(k;m) & \Delta_{22}^F(k;m)\end{pmatrix}U(k)^{-1}=\begin{pmatrix}\Delta_0^F(k;m) & 0\\ 0 & -\Delta_0^F(k;m)^*\end{pmatrix}, \tag{A10}$$

where $\Delta_0^F(k;m)$ is the Feynman propagator at $T=0$,

$$\Delta_0^F(k;m)=\frac{1}{k^2-m^2+i\eta}. \tag{A11}$$

It is known that $U(k)$ also diagonalizes the full propagator [19] as well as $\Pi_{ab}(k)$

$$\Pi_{ab}(k)=[U(k)^{-1}]_{ac}\begin{pmatrix}\overline{\Pi}(k) & 0\\ 0 & -\overline{\Pi}(k)^*\end{pmatrix}_{cd}[U(k)^{-1}]_{db}. \tag{A12}$$

This matrix equation gives relations between matrix elements:

$$\mathrm{Re}\,\overline{\Pi}(k)=\mathrm{Re}\,\Pi_{11}(k), \tag{A13}$$

$$\mathrm{Im}\,\overline{\Pi}(k)=\tanh(\beta|k_0|/2)\,\mathrm{Im}\,\Pi_{11}(k), \tag{A14}$$

$$\mathrm{Im}\,\overline{\Pi}(k)=i\sinh(\beta|k_0|/2)\Pi_{12}(k). \tag{A15}$$

Let us next find the expression of the spectral function. Δ_{11} has the following spectral representation:

$$\Delta_{11}(k;m)=\int \mathrm{d}\omega^2\rho(\omega,\mathbf{k})\Delta_{11}^F(k_0,\omega), \tag{A16}$$

where we denote the argument of Δ_{11}^F by k_0 and $\omega\equiv\sqrt{\mathbf{k}^2+m^2}$ instead of k and m. One can prove that, if Δ_{11} is given in Eq. (A16), the Green function

$$\Delta(t,\mathbf{x})=\frac{i}{(2\pi)^4}\int \mathrm{d}^4k e^{ik\cdot x}\Delta_{11}(k;m) \tag{A17}$$

obeys the Kubo-Martin-Schwinger (KMS) condition [31]. From Eq. (A16) we obtain

$$\rho(k) = -\frac{1}{\pi}\tanh(\beta|k_0|/2)\,\mathrm{Im}\,\Delta_{11}(k;m). \tag{A18}$$

Our next task is thus to find the expression of $\mathrm{Im}\,\Delta_{11}(k;m)$. Denoting the diagonalized full propagator by

$$U(k)^{-1}\tilde{\Delta}(k;m)U(k)^{-1} = \begin{pmatrix} \Delta(k;m) & 0 \\ 0 & -\Delta(k;m)^* \end{pmatrix}, \tag{A19}$$

we obtain

$$\begin{aligned}\tilde{\Delta} &= U(k)\begin{pmatrix} \Delta(k;m) & 0 \\ 0 & -\Delta(k;m)^* \end{pmatrix} U(k) \\ &= \begin{pmatrix} [1+n(k_0)]\Delta(k;m) - n(k_0)\Delta(k;m)^* & \sqrt{n(k_0)[1+n(k_0)]}[\Delta(k;m)-\Delta(k;m)^*] \\ \sqrt{n(k_0)[1+n(k_0)]}[\Delta(k;m)-\Delta(k;m)^*] & -[1+n(k_0)]\Delta(k;m)^* + n(k_0)\Delta(k;m) \end{pmatrix}.\end{aligned} \tag{A20}$$

Taking the (1,1) components in both sides of the above equation yields

$$\mathrm{Im}\,\Delta_{11}(k;m) = \coth(\beta|k_0|/2)\,\mathrm{Im}\,\Delta(k;m). \tag{A21}$$

The expression for $\Delta(k;m)$ can be found in the following manner. In Eq. (A8), iteratively using Eq. (A8) itself in the right-hand side and diagonalizing, we obtain

$$\begin{aligned} U(k)^{-1}&\tilde{\Delta}(k;m)U(k)^{-1} \\ &= \begin{pmatrix} \Delta_0^F(k;m) & 0 \\ 0 & -\Delta_0^F(k;m)^* \end{pmatrix} \\ &\quad + \begin{pmatrix} \Delta_0^F(k;m) & 0 \\ 0 & -\Delta_0^F(k;m)^* \end{pmatrix} \\ &\quad \times \begin{pmatrix} \overline{\Pi}(k) & 0 \\ 0 & -\overline{\Pi}(k)^* \end{pmatrix} \\ &\quad \times \begin{pmatrix} \Delta_0^F(k;m) & 0 \\ 0 & -\Delta_0^F(k;m)^* \end{pmatrix} + \cdots. \end{aligned} \tag{A22}$$

The (1,1) component of this equation gives

$$\begin{aligned}\Delta(k;m) &= [U(k)^{-1}\tilde{\Delta}(k;m)U(k)^{-1}]_{11} \\ &= \Delta_0^F(k;m) + \Delta_0^F(k;m)\overline{\Pi}(k)\Delta_0^F(k;m) + \cdots \\ &= \frac{1}{k^2 - m^2 - \overline{\Pi}(k)}.\end{aligned} \tag{A23}$$

Therefore, from Eqs. (A18), (A21), and (A23), we obtain the desired expression of the spectral function:

$$\rho(k) = -\frac{1}{\pi}\frac{\mathrm{Im}\,\overline{\Pi}(k)}{[k^2 - m^2 - \mathrm{Re}\,\overline{\Pi}(k)]^2 + [\mathrm{Im}\,\overline{\Pi}(k)]^2}. \tag{A24}$$

Thus the spectral function can be written only with one component of the self-energies while all the components enter $\Delta_{11}(k;m)$ [see Eq. (A8)].

APPENDIX B: STRUCTURE OF THE IMAGINARY PART OF THE SUNSET DIAGRAM

In this appendix we study the structure of the imaginary part of the sunset diagram. We rederive the results of [3–5] by extending the method for bubble diagrams by Fujimoto *et al.* [32]. Following the method by the authors, we use Eq. (A15) [32], namely

$$\begin{aligned}\mathrm{Im}\,i\overline{\mathcal{I}}_{\mathrm{sun}}&(k;m_1,m_2,m_3) \\ &= i\sinh(\beta|k_0|/2)\,i\mathcal{I}_{\mathrm{sun}}(k;m_1,m_2,m_3)_{12}.\end{aligned} \tag{B1}$$

Here $\overline{\mathcal{I}}_{\mathrm{sun}}(k;m_1,m_2,m_3)$ is the (1,1) component of the diagonalized self-energy matrix for the sunset diagram in real time formalism, and $\beta \equiv 1/T$ (T is temperature). We note that the self-energy which actually enters spectral functions is the diagonalized one [see Eq. (A24)]. $\mathcal{I}_{\mathrm{sun}}(k;m_1,m_2,m_3)_{12}$ is the (1,2) component of the sunset diagram, which is given by the following integral:

$$\begin{aligned}i\mathcal{I}_{\mathrm{sun}}(k;m_1,m_2,m_3)_{12} &= \int \frac{\mathrm{d}^4p}{(2\pi)^4} i\Delta_{12}^F(p;m_1) \\ &\quad \times i\mathcal{I}_{\mathrm{bub}}(k-p;m_2,m_3)_{12},\end{aligned} \tag{B2}$$

where $\Delta_{12}^F(p;m)$ is the (1,2) component of the free propagator whose expression is given in Eq. (A6). Here, it is convenient to use its another form:

$$i\Delta_{12}^{F}(p;m_1)=e^{\beta p_0/2}f(p_0)\epsilon(p_0)2\pi\delta(p^2-m_1^2),$$

$$f(p_0)=\frac{1}{e^{\beta p_0}-1}. \tag{B3}$$

$i\mathcal{I}_{\rm bub}(p;m_1,m_2)_{12}$ denotes the (1,2) component of the bubble diagram:

$$i\mathcal{I}_{\rm bub}(k-p;m_2,m_3)_{12} =i\int\frac{d^4q}{(2\pi)^4}i\Delta_{12}^{F}(q;m_2)i\Delta_{12}^{F}(k-p-q;m_3). \tag{B4}$$

One can reduce this equation to

$$\begin{aligned} i\mathcal{I}_{\rm bub}(p;m_1,m_2)_{12}=&ie^{\beta(k_0-p_0)/2}f(k_0-p_0)\\ &\times\int\frac{d^4q}{(2\pi)^2}\frac{1}{4E_2E_3}\{(1+n_2+n_3)[\delta(k_0\\ &-p_0-E_2-E_3)-\delta(k_0-p_0-E_2+E_3)]\\ &-(n_2-n_3)[\delta(k_0-p_0-E_2+E_3)\\ &-\delta(k_0-p_0+E_2-E_3)]\}, \end{aligned} \tag{B5}$$

where $E_2=\sqrt{|\mathbf{q}|^2+m_2^2}$ and $E_3=\sqrt{|\mathbf{k}-\mathbf{p}-\mathbf{q}|^2+m_3^2}$. We also define $E_1=\sqrt{|\mathbf{p}|^2+m_1^2}$ for later use. n_i is the Bose-Einstein factor defined by $n_i=n(E_i)=1/(e^{\beta E_i}-1)$. Using Eqs. (B1) and (B2) in which Eq. (B5) is substituted yields

$$\begin{aligned} \mathrm{Im}\,i\bar{\mathcal{I}}_{\rm sun}(k;m_1,m_2,m_3) =&-\pi\epsilon(k_0)\int\frac{d^3p}{(2\pi)^3}\int\frac{d^3q}{(2\pi)^3}\frac{1}{8E_1E_2E_3}\{[(1+n_1)\\ &\times(1+n_2)(1+n_3)-n_1n_2n_3]\delta(k_0-E_1-E_2-E_3)\\ &+[n_1n_2n_3-(1+n_1)(1+n_2)(1+n_3)]\delta(k_0+E_1\\ &+E_2+E_3)+([n_2n_3(1+n_1)-n_1(1+n_2)(1+n_3)]\\ &\times\delta(k_0-E_1+E_2+E_3)+[n_1(1+n_2)(1+n_3)\\ &-n_2n_3(1+n_1)]\delta(k_0+E_1-E_2-E_3)\\ &+(\text{permutations}))\}. \end{aligned} \tag{B6}$$

In this equation "permutations" stands for the terms obtained by permuting the particle labels of the third and the forth terms.

Let us now consider the physical content of Eq. (B6). The first term in Eq. (B6) may be interpreted as the probability for the decay $\Phi\to\phi_1\phi_2\phi_3$ with the statistical weight $(1+n_1)(1+n_2)(1+n_3)$ for stimulated emission minus the probability for the creation $\phi_1\phi_2\phi_3\to\Phi$ with the weight $n_1n_2n_3$ for absorption. The second term is the antiparticle counterpart of the first term. The third term represents the probability for $\Phi\bar{\phi}_2\bar{\phi}_3\to\phi_1$ with the weight $n_2n_3(1+n_1)$ minus that for $\phi_1\to\Phi\bar{\phi}_2\bar{\phi}_3$ with the weight $n_1(1+n_2)(1+n_3)$. Here $\bar{\phi}_i$ stands for the antiparticle of ϕ_i. The forth term is the antiparticle counterpart of the third term. It represents the probability for $\Phi\bar{\phi}_1\to\phi_2\phi_3$ with the weight $n_1(1+n_2)(1+n_3)$ minus that for $\phi_2\phi_3\to\Phi\bar{\phi}_1$ with the weight $n_2n_3(1+n_1)$. All processes are shown in Fig. 9.

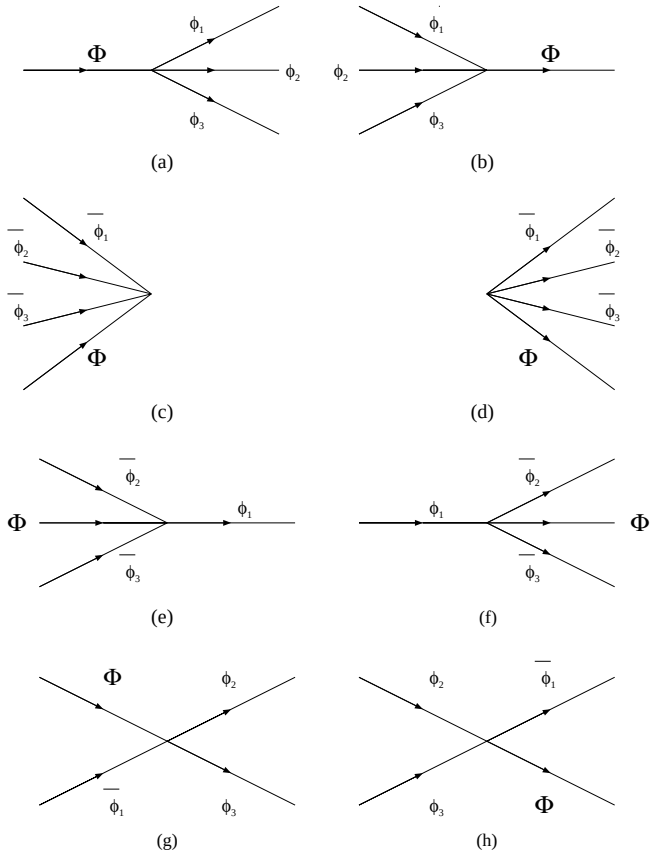

FIG. 9. The amplitudes in Eq. (B6) responsible for the disappearance and reappearance of Φ. $\bar{\phi}_i$ stands for an antiparticle of ϕ_i. (a) minus (b) corresponds to the first term in Eq. (B6), (c) minus (d) to the second, (e) minus (f) to the third, and (g) minus (h) to the forth. Amplitudes obtained by permuting particle labels of (e), (f), (g), and (h) also exist.

We next find the region of k^2 where the physical processes contained in Eq. (B6) are possible, which is equivalent to looking for the condition under which the integral over q in Eq. (B6) survives. For the first and the second terms in Eq. (B6) to be nonvanishing, k^2 must satisfy the condition $k^2>(m_1+M_{23})^2$, where M_{23} is the invariant mass of ϕ_2 and ϕ_3. Therefore, the processes in Figs. 9(a)–9(d) are possible for $k^2>(m_1+m_2+m_3)^2$ since $M_{23}>m_2+m_3$. The third and the fourth terms survive when $k^2<(m_1-M_{23})^2$. The processes in Figs. 9(e)–9(h), therefore, take place at arbitrary k^2. This is reasonable since the processes in Figs. 9(g) and 9(h) are scattering ones and since those in Figs. 9(e) and 9(f) can be also regarded as scattering by interpreting the incoming Φ in (e) as an outgoing anti-Φ and by doing the outgoing Φ in (f) as an incoming anti-Φ. Accordingly, the imaginary part of the sunset diagram is nonvanishing for arbitrary k^2, which is a remarkable feature of the thermal self-energy at and beyond two-loop order [3,5].

[1] S. Chiku and T. Hatsuda, Phys. Rev. D **57**, R6 (1998); **58**, 076001 (1998).
[2] J.O. Andersen, E. Braaten, and M. Strickland, Phys. Rev. D **63**, 105008 (2001), and references therein.
[3] S. Jeon, Phys. Rev. D **52**, 3591 (1995).
[4] E. Wang and U. Heinz, Phys. Rev. D **53**, 899 (1996).
[5] J.P. Blaizot and E. Iancu, Phys. Rep. **359**, 355 (2002).
[6] H. van Hees and J. Knoll, Phys. Rev. D **65**, 105005 (2002).
[7] J. Schwinger, J. Math. Phys. **2**, 407 (1961).
[8] L.V. Keldysh, Sov. Phys. JETP **20**, 1018 (1964).
[9] R.A. Craig, J. Math. Phys. **9**, 605 (1968).
[10] G.-Z. Zhou, Z.-B. Su, B.-L Hao, and L. Yu, Phys. Rev. B **22**, 3385 (1980).
[11] Y. Takahashi and H. Umezawa, Collect. Phenom. **2**, 55 (1975).
[12] G.W. Semenoff and Y. Takahashi, Nucl. Phys. **B220**, 196 (1983).
[13] L.P. Kadanoff and G. Baym, *Quantum Statistical Mechanics* (Benjamin, New York, 1969); D.C. Langreth, in *1975 NATO ADI on Linear and Non-Linear Electron Transport in Solids*, edited by J.T. Devreese and E. van Boem (Plenum, New York, 1976).
[14] R. Mills, *Propagators for Many-Particle Systems* (Gordon and Breach, New York, 1969).
[15] E.M. Lifshitz and L.P. Pitaevskii, *Course of Theoretical Physics, Vol. 10*: *Physical Kinetics* (Pergamon, New York, 1981).
[16] H. Umezawa, H. Matsumoto, and M. Tachiki, *Thermofield Dynamics and Condensed States* (North-Holland, Amsterdam, 1982).
[17] A.J. Niemi and G.W. Semenoff, Ann Phys. **B152**, 105 (1984).
[18] A.J. Niemi and G.W. Semenoff, Nucl. Phys. **B230**, 181 (1984).
[19] M. Lebellac, *Thermal Field Theory* (Cambridge University Press, Cambridge, England, 1996).
[20] H.A. Weldon, Phys. Rev. D **28**, 2007 (1983).
[21] See, for example, P. Ramond, *Field Theory, A Modern Primer* (Benjamin/Cummings, New York, 1981).
[22] P. Post and J.B. Tausk, Mod. Phys. Lett. A **11**, 2115 (1996).
[23] J. Gasser and M.E. Sainio, Eur. Phys. J. C **6**, 297 (1999).
[24] J.O. Andersen and E. Braaten, Phys. Rev. D **62**, 045004 (2000); E. Braaten and A. Nieto, *ibid.* **51**, 6990 (1995).
[25] S. Groote, J.G. Körner, and A.A. Pivovarov, Phys. Lett. B **443**, 269 (1998); Nucl. Phys. **B542**, 515 (1999); Eur. Phys. J. C **11**, 279 (1999).
[26] S. Weinberg, Phys. Rev. D **9**, 3357 (1974); L. Dolan and R. Jackiw, *ibid.* **9**, 3320 (1974).
[27] D.A. Kirzhnits and A.D. Linde, Ann. Phys. (N.Y.) **101**, 195 (1976).
[28] Y. Hidaka, O. Morimatsu, T. Nishikawa, and M. Ohtani, hep-ph/0304204.
[29] T. Nishikawa, O. Morimatsu, and Y. Hidaka (in preparation).
[30] M.E. Peskin and D.V. Schroeder, *An Introduction to Quantum Field Theory* (Perseus Books, Cambridge, MA, 1995).
[31] G.W. Semenoff and H. Umezawa, Nucl. Phys. **B220**, 196 (1983).
[32] Y. Fujimoto, M. Morikawa, and M. Sasaki, Phys. Rev. D **33**, 590 (1986).